Influence of the fibre laser parameters on the surface texturing of 420 stainless steel

Ângela Cunha (angelacunha1994@gmail.com)
University of Minho School of Engineering: Universidade do Minho Escola de Engenharia
https://orcid.org/0000-0003-0610-6255
Ana Marques
Flávio Bartolomeu
Filipe Samuel Silva
Michael Gasik
Bruno Trindade
Óscar Carvalho

Research Article

Keywords: 420 stainless steel, laser surface texturing, laser parameters, microstructure, hardness

Posted Date: February 8th, 2022

DOI: https://doi.org/10.21203/rs.3.rs-1317794/v1

Abstract

The surface of an annealed 420 stainless steel plate was textured using a fibre laser in this work. Four hundred textures were produced from eighty different combinations of processing parameters (laser power, scan speed, line spacing and number of passes). The most promising textures (fourteen combinations of the processing parameters) were obtained with laser power values of 16 and 64 %, scanning speeds up to 2,000 mm/s, number of passes of 8 or higher and line spacings of 40 and 50 µm. The lower the laser power, the lower the scanning speed and the high number of passes and line spacings were required for a suitable ablation process. High laser powers were responsible for the dissolution of the chromium carbides in the laser tracks (top and edges of the unmachined areas). The hardness of these regions was 320 ± 11 HV against 255 ± 5 HV for the unmachined zones.

1. Introduction

AISI 420 martensitic stainless steel is a material widely used in the mould industry as well as having other tooling applications such as surgical tools [1–3] due to its high tensile strength, hardness, and corrosion properties [1–5]. In the annealing state, its structure consists of a ferritic matrix with a homogeneous dispersion of $M_{23}C_6$ spheroidised carbides with a high ductility [3]. The tensile strength and hardness properties are improved by a quenching heat treatment in which a martensite structure is formed [3]. The presence of alloyed chromium increases the corrosion resistance [1, 6]. However, this material has some limitations where good tribological properties are required, i.e. where controlled friction, and increased wear resistance and lubrication are needed.

Different approaches have been used to modify the surface properties of steel components such as sandblasting, chemical etching, deposition of coatings, electrode discharge machining (EDM), electrochemical machining (ECM), and texturing by electron beam, electric arc, or laser ablation [7–10]. Laser surface texturing, in particular, has been an efficient surface modification technique to improve the thermal efficiency of components, as well as their tribological behaviour [11, 12]. However, just one study on the laser surface texturing of 420 stainless steel was found in the literature. In that study, Pan *et al.* [13] used a picosecond laser for the fabrication of a superhydrophobic antibacterial textured surface on 420 stainless steel plates.

Several types of lasers such as CO_2 (10.64 µm), YAG (1064 nm) and diode (848 nm) can be used for machining or to texture surfaces. The type of laser and wavelength to be used for a specific application must be selected according to the material to be textured since it influences the energy absorbed [14, 15].

This work concerns the texturing of a 420 stainless steel by an Nd: YVO_4 fibre laser. A detailed study of the influence of the laser parameters on the quality of the textures produced is presented and discussed. Four hundred textures were produced from eighty different combinations of processing parameters (power, scan speed, and number of passes).

2. Experimental Procedure

Square 420 stainless steel (35 mm · 3 mm) samples were textured using an Nd: YVO_4 fibre laser (Model XM-30D Fibre Laser Marking Machine) with a wavelength of 1,064 nm, maximum power of 30 W, spot size of 10 µm, and pulse width of 10 µs. The processing parameters (laser and drawing parameters) used in this work are shown in Table 1. The texturisation process is presented in Figure 1. The number of lines varied from 10 to 50 depending on the drawing parameters. The greater the line spacing the lower the number of lines.

Table 1
Summary of the processing parameters used for the laser machining of the 420 stainless steel surface.

Laser parameters			**Drawing parameters**
Laser power - *P* (%)	Scan speed - *s* (mm/s)	Number of passes - *n*	Line spacing - *l* (µm)
1 (0.3 W)	100	1	10
16 (4.8 W)	500	8	20
64 (19.2 W)	2,000	32	30
100 (30 W)	5,000	128	40
		256	50

The set of parameters presented in Table 1 correspond to different laser energy fluences (*F*), defined as the laser energy divided by the area (J/mm^2). This parameter is calculated considering the laser power (P) in W, the scanning speed (s) in mm/s, the number of passes/loops (n), and the line spacing/interspacing between adjacent lines (l) in mm, according to the equation:

$$F = \frac{P}{s \times l} \times n$$

In this work, the laser energy fluence value varied from ~0 to 7,680 J/mm^2.

The dimensional/topological analysis of the textures (surface width and depth of the grooves) was done using the scanning electron microscopy (SEM) images (NanoSEM-FEI Nova 200 (FEG/SEM)), by means of an image analysis software (Image J), and by 3D profilometry (InfiniteFocus from Bruker alicona).

Prior to the observations, the samples were polished with silicon carbide abrasive papers with successive grades till 4,000 mesh. The influence of the laser parameters on the microstructure and grain size of the 420 stainless steel was assessed by optical metallography after etching the samples with Vilella's reagent. X-ray diffraction (XRD) (PANalytical X'Pert PRO MPD with Co Kα radiation) was used for the structural analysis. Hardness of the samples was evaluated by means of Shimadzu HMV-2 equipment with a load of 10 gf and a dwell time of 15 s.

3. Results And Discussion

Raw material

The raw 420 stainless steel plate was formed by ferrite and spheroidised chromium carbides (Fig. 2), characteristic of an annealed state.

Texturing

Figure 3 shows the SEM images of the textured 420 stainless steel produced with different processing parameters. The quality of the textures was evaluated considering two factors: continuity of the machined grooves and dimension of cavities produced. Fourteen different combinations of processing parameters were found to give rise to continuous textures (marked in red in Fig. 3). Another fourteen conditions (marked in yellow) corresponding to low laser powers and high scanning speed did not reveal any visible cavities using SEM cross-section analysis, probably due to the accumulation of material at the site where the supposed laser ablation occurs or lack of removal capacity (low laser energy fluence) [16, 17].

The definition and quality of the grooves depends on the processing parameters. For low laser powers, low scanning speeds and a high number of passes and line spacings are required for a suitable ablation process. Low laser powers (1 and 16%) combined with high scan speeds (2,000 and 5,000 mm/s), and line spacings of 40 and 50 µm, led to low-quality and non-uniform textures, characterised by discrete machined areas (Fig. 4a). This phenomenon is due to the low laser energy fluence obtained for these parameter combinations. Furthermore, for low laser power (1%) and mainly for a low number of passes, it is possible to observe a continuous action of the laser, but non-machined areas are also observed (Fig. 4b). Average power laser values of 16 and 64%, scanning speeds up to 2,000 mm/s, 8 passes or more and line spacings of 40 and 50 µm gave rise to the largest number of good quality grooves (Fig. 4c). In fact, the definition of the machined lines increased as the line spacing increased, because of the reduced interaction between successive passes of the laser.

For the maximum laser power (100%), high scanning speeds and greater line spacings are required to produce suitable textures. The number of passes plays an important role in this case: for n = 1, the tracks are shallow whilst for n > 8 an excessive remelting of the base material occurs. The high energy leads to an exaggerated increase in the surface temperature, which causes the material around the area being irradiated by the laser to melt, therefore impeding its ablation. This phenomenon was also detected for high laser powers and low scan speeds and leads to some material accumulating inside the grooves. This is particularly true for a high number of passes (Fig. 5).

In fact, the amount of laser energy absorved by the material decreases significantly throughout the thickness and has a great influence on the surface outcome. Therefore, if the energy is high enough the material is ablated, and it creates a textured surface. This may occur when combining medium to high laser power with a medium scan speed. On the other hand, a remelted surface occurs when the amount

of energy is insufficient for ablation or is too high and causes the material to overheat, which occurs when high laser powers and low scan speeds are used.

The morphology of the abovementioned fourteen promising textures was analysed by 3D profilometry (Fig. 6). The corresponding width and depth values were determined in the middle of the textured grooves and are presented in Figure 7.

From Figures 6 and 7 it is possible to conclude that: (i) the groove width grows with the increase in the number of passes for medium and high laser powers and scanning speeds (16-64% and 500-2,000 mm/s, respectively). For low laser powers (1%) and scanning speeds (100 mm/s), increasing the number of passes is no longer beneficial to increase the width. Regarding the depth, as expected, it tends to increase with the number of passes; (ii) the increase in laser power has a significant impact on width and depth (cases analysed: *P*64 *s*2,000 *n*8 *l*50 and *P*100 *s*2,000 *n*8 *l*50). The percentage difference verified in the case of the width is 20% while in the case of the depth it is 16%; (iii) in the case of scanning speed, two cases could be analysed: the use of low scanning speeds (100 and 500 mm/s) and the use of high scanning speeds (2,000 and 5,000 mm/s). In the former, the increase in scanning speed led to a sharp decrease in width, while in the latter the variation in width is inverse. On the other hand, in the case of depth, a low scanning speed has a no significant impact while a high scanning speed increases this value. Therefore, for low laser powers (16%) and scanning speeds (100 and 500 mm/s), increasing the scanning speed has a strong negative impact on width, whereas for high laser powers (100%) and scanning speeds (2,000 and 5,000 mm/s), increasing the scanning speed has a strong positive impact on width; (iv) The line spacing proved not to be a determinant factor regarding the width and depth of the textured grooves for the parameters studied.

(*P* = laser power in %, *s* = scanning speed in mm/s, *n* = number of passes, *l* = line spacing in μm)

Figure 8 shows the SEM images of the cross-section of the grooves. For low laser powers (1 and 16%), the grooves produced present a waveform, with no noticeable differences when the other parameters are changed (scan speed, number of passes, and line spacing). On the other hand, when the laser power is increased (64 and 100%) the cavity has a more defined shape. In this case, the increase in the number of passes led to the formation of a cavity with a more funneled shape. Therefore, it is possible to conclude that the width, depth, and shape of the cavities are influenced not only by the laser energy fluence but also by each individual process parameter. For the same laser energy fluence values, the change in laser power and scanning speed was shown to affect these cavities' characteristics significantly (width, depth, and shape). Comparing the results obtained by 3D profilometry and SEM (Figs. 7 and 8, respectively), a discrepancy in width and, mainly, depth of the grooves is observed. This can be explained by Figure 9 which shows that the depth of the cavity along the groove is not constant, it is greater at the beginning of the ablation process. This is due to the excessive increase in the surface temperature and with the formation of a great amount of the liquid phase that impedes the penetration of the laser beam and consequent ablation of the material.

The influence of the processing parameters on the microstructure of the different textured samples was assessed by optical metallography from their cross-section. Figure 10 shows the two typical examples of textures obtained from different processing parameters.

For low laser powers, the scanning speed did not influence the microstructure of the base material (Fig. 10a), formed by ferrite + chromium carbides. However, for higher laser power values, and number of passes higher than 1, white regions with no carbides could be detected on the top and the edges of the unmachined areas, corresponding to remelted base material (Fig. 10b). This means that high laser powers are responsible for the dissolution of the chromium carbides. Microhardness evaluation was performed in these regions and far from the machined tracks. Values of 320 ± 11 HV and 255 ± 5 HV were obtained, respectively. The dissolution of the chromium carbides led to the incorporation of chromium in the austenite at a high temperature with the corresponding hardening of the microstructure after cooling.

4. Conclusions

An Nd: YVO4 fibre laser was successfully used to texture an annealed 420 stainless steel plate. The following main conclusions can be drawn from this study:

- The processing parameters influenced the ablation process.
- The most promising textures were obtained with laser power values of 16 and 64%, scanning speeds of up to 2,000 mm/s, number passes of 8 or higher and line spacings of 40 and 50 μm.
- For low values of laser power, low scanning speeds and a high number of passes and greater line spacings were required to obtain a good quality texture. The inverse situation was observed for high laser power values, which was responsible for microstructural changes on the top and edges of the regions adjacent to the machined ones (chromium carbide dissolution), with an increase in hardness.

Declarations

Funding

This work is supported by FCT (Fundação para a Ciência e a Tecnologia) through the grant SFRH/BD/147460/2019 and the project POCI-01-0247-FEDER-024533. Additionally, this work is supported by FCT national funds, under the national support to R&D units grants, through the reference projects UIDB/04436/2020 and UIDP/04436/2020, and UIDB/00285/2020.

Conflicts of interests/Competing interests

The authors declare that they have no known competing financial interests or personal relationships that could have appeared to influence the work reported in this paper.

Availability of data and material

Data available on request from the authors. The data that supported the findings of this study are available from the corresponding author, Ângela Cunha, upon reasonable request.

Code availability

Not applicable.

Ethics approval

Not applicable.

Consent to participate

The authors declare that all authors have approved the manuscript and agree with its submission to IJAMT.

Consent for publication

The authors declare that all authors agree to sign the transfer of copyright for the publisher to publish this article upon on acceptance.

Author's contributions

Ângela Cunha: Methodology, Validation, Investigation, Writing - Original Draft

Ana Marques: Methodology, Investigation

Flávio Bartolomeu: Writing - Review & Editing

Filipe Samuel Silva: Conceptualization, Validation, Supervision

Michael Gasik: Writing- Review and Editing

Bruno Trindade: Investigation, Validation, Writing - Review & Editing

Óscar Carvalho: Conceptualization, Investigation, Supervision, Writing - Review & Editing

References

1. Saeidi K, Zapata DL, Lofaj F et al (2019) Ultra-high strength martensitic 420 stainless steel with high ductility. Addit Manuf 29:100803. https://doi.org/10.1016/j.addma.2019.100803
2. Nath SD, Clinning E, Gupta G et al (2019) Effects of Nb and Mo on the microstructure and properties of 420 stainless steel processed by laser-powder bed fusion. Addit Manuf 28:682–691. https://doi.org/10.1016/j.addma.2019.06.016

3. Nath SD, Irrinki H, Gupta G et al (2019) Microstructure-property relationships of 420 stainless steel fabricated by laser-powder bed fusion. Powder Technol 343:738–746. https://doi.org/10.1016/j.powtec.2018.11.075
4. Nath SD, Gupta G, Kearns M et al (2020) Effects of layer thickness in laser-powder bed fusion of 420 stainless steel. Rapid Prototyp J 26:1197–1208. https://doi.org/10.1108/RPJ-10-2019-0279
5. Momenzadeh N, Nath SD, Berfield TA, Atre SV (2019) In Situ Measurement of Thermal Strain Development in 420 Stainless Steel Additive Manufactured Metals. Exp Mech 59:819–827. https://doi.org/10.1007/s11340-019-00513-3
6. Nachum S, Fleck NA (2011) The microstructure and mechanical properties of ball-milled stainless steel powder: The effect of hot-pressing vs. laser sintering. Acta Mater 59:7300–7310. https://doi.org/10.1016/j.actamat.2011.08.004
7. Babu V, Yaradi M, Thammineni DT (2018) A Review on Recent Trends in Surface Coatings
8. Horodek P, Eseev MK, Kobets AG (2015) Studies of stainless steel exposed to sandblasting. Nukleonika 60:721–724. https://doi.org/10.1515/nuka-2015-0129
9. Ormanova M, Petrov P, Kovacheva D (2016) Electron beam surface treatment of tool steels. https://doi.org/10.1016/j.vacuum.2016.10.022. Vacuum
10. Arslan A, Masjuki HH, Kalam MA et al (2016) Surface Texture Manufacturing Techniques and Tribological Effect of Surface Texturing on Cutting Tool Performance: A Review. Crit Rev Solid State Mater Sci 41:447–481. https://doi.org/10.1080/10408436.2016.1186597
11. Kumar V, Verma R, Kango S, Sharma VS (2021) Recent progresses and applications in laser-based surface texturing systems. Mater Today Commun 26:101736. https://doi.org/10.1016/j.mtcomm.2020.101736
12. Amoroso PJ, Ramalho A, Richhariya V et al (2021) Tribological performance of laser-textured steel surfaces in unidirectional sliding line-contact (block-on-ring). Lubr Sci 1–15. https://doi.org/10.1002/ls.1563
13. Pan Q, Cao Y, Xue W et al (2019) Picosecond Laser-Textured Stainless Steel Superhydrophobic Surface with an Antibacterial Adhesion Property. Langmuir 35:11414–11421. https://doi.org/10.1021/acs.langmuir.9b01333
14. Fatoba OS, Popoola PAI, Pityana SL, Adesina OS (2016) Computational Dynamics of Anti-Corrosion Performance of Laser Alloyed Metallic Materials. In: Fiber Laser
15. Pereira H, Carvalho O, Miranda G, Silva FS (2020) Pure magnesium laser surface modification using Nd:YAG laser. Mater Technol 1–5. https://doi.org/10.1080/10667857.2020.1797326
16. Lickschat P, Metzner D, Weißmantel S (2020) Fundamental investigations of ultrashort pulsed laser ablation on stainless steel and cemented tungsten carbide. Int J Adv Manuf Technol 109:1167–1175. https://doi.org/10.1007/s00170-020-05502-8
17. Hazzan KE, Pacella M, See TL (2021) Laser processing of hard and ultra-hard materials for micro-machining and surface engineering applications. Micromachines 12. https://doi.org/10.3390/mi12080895

Figures

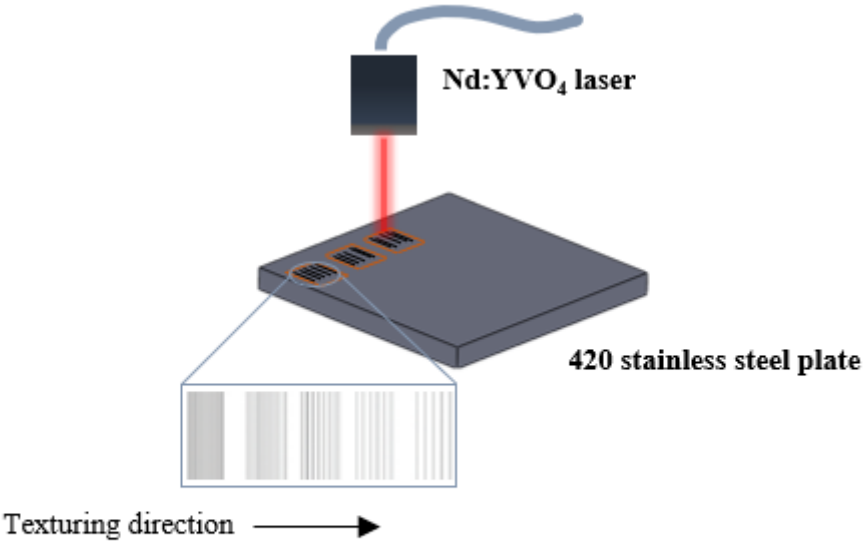

10	20	30	40	50	Line spacing (µm)
50	25	17	13	10	Number of lines

Figure 1

Texturisation process: laser strategy with a different number and spacing of lines.

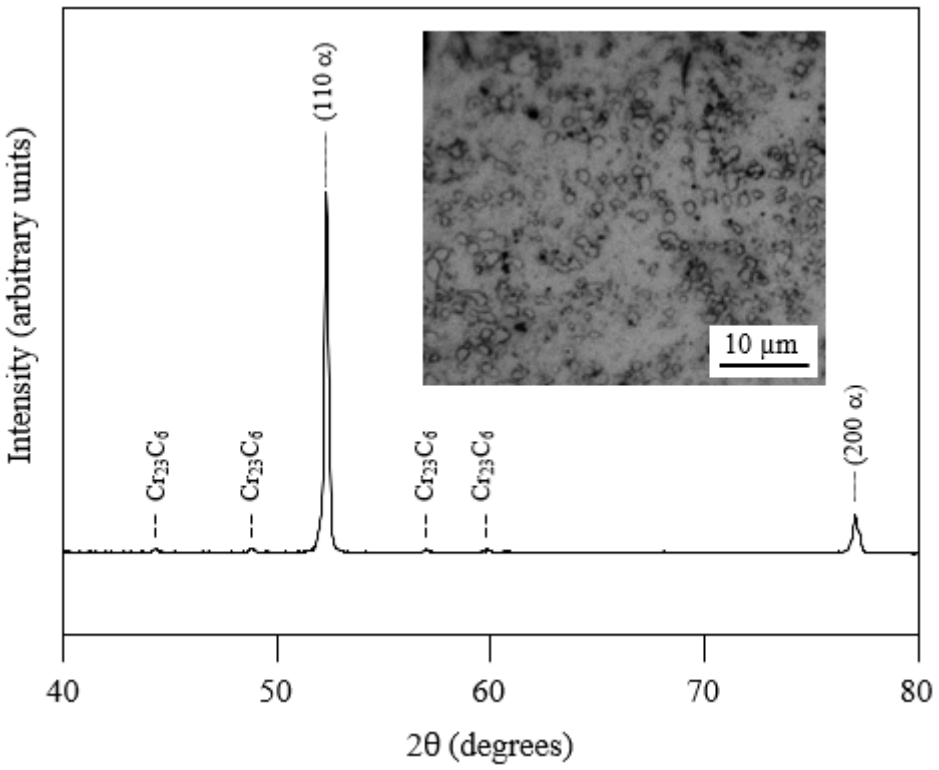

Figure 2

XRD pattern and optical micrograph of the microstructure of a raw 420 stainless steel plate.

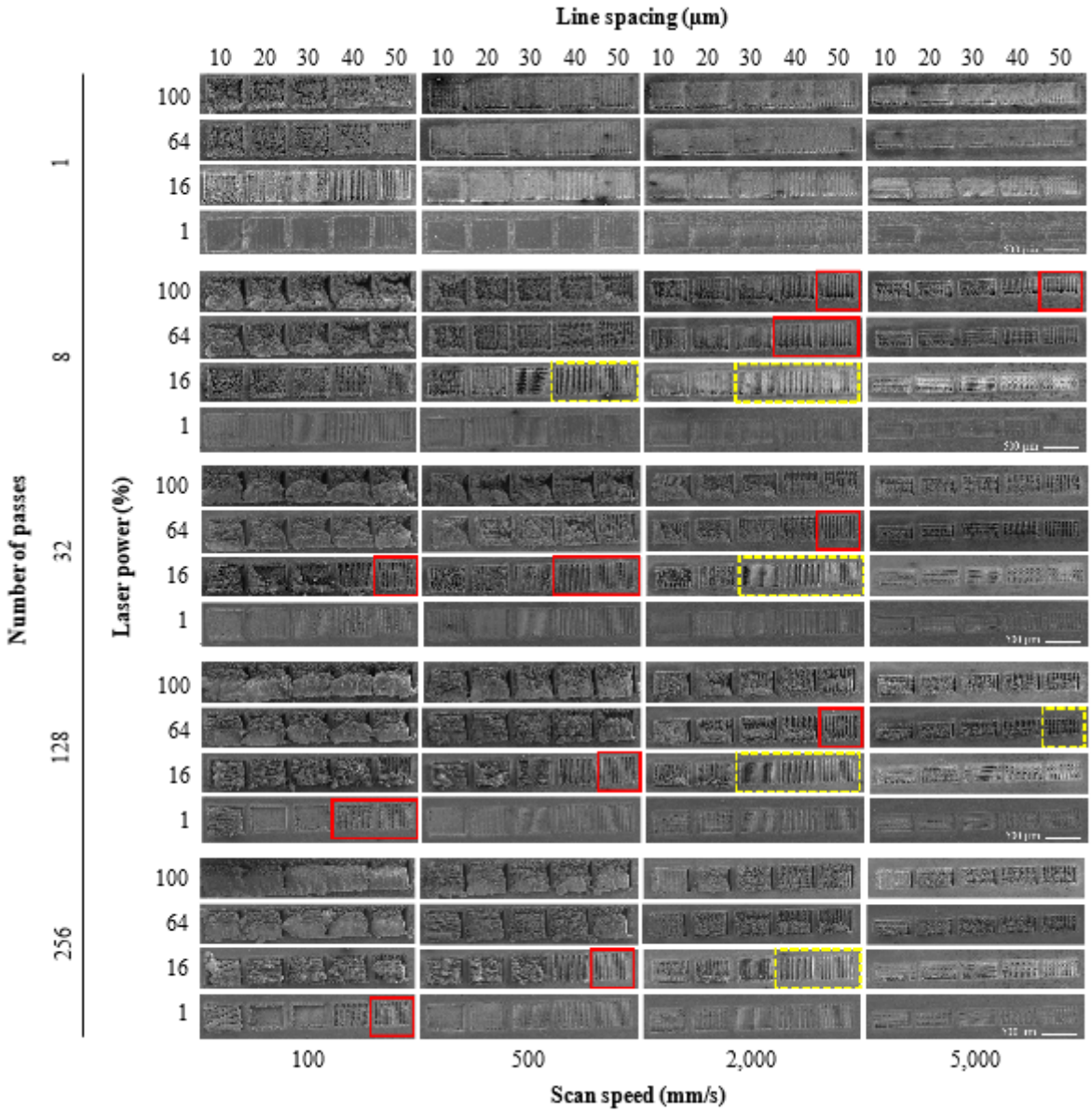

Figure 3

SEM images of the 420 stainless steel textured samples processed with different processing parameters (laser power, scan speed, number of passes and line spacing).

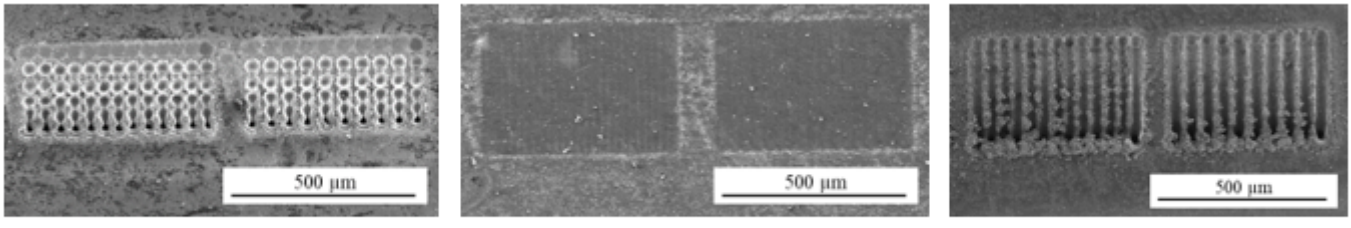

Figure 4

Example of different phenomena that occur during texturing: (a) laser spot separation - discrete machined areas (P = 16 %, s = 5,000 mm/s, n = 8, l = 40 and 50 µm), (b) insufficient machining (P = 1 %, s = 500 mm/s, n = 1, l = 20 and 30 µm), and (c) adequate machining (P = 64 %, s = 2,000 mm/s, n = 8, l = 40 and 50 µm).

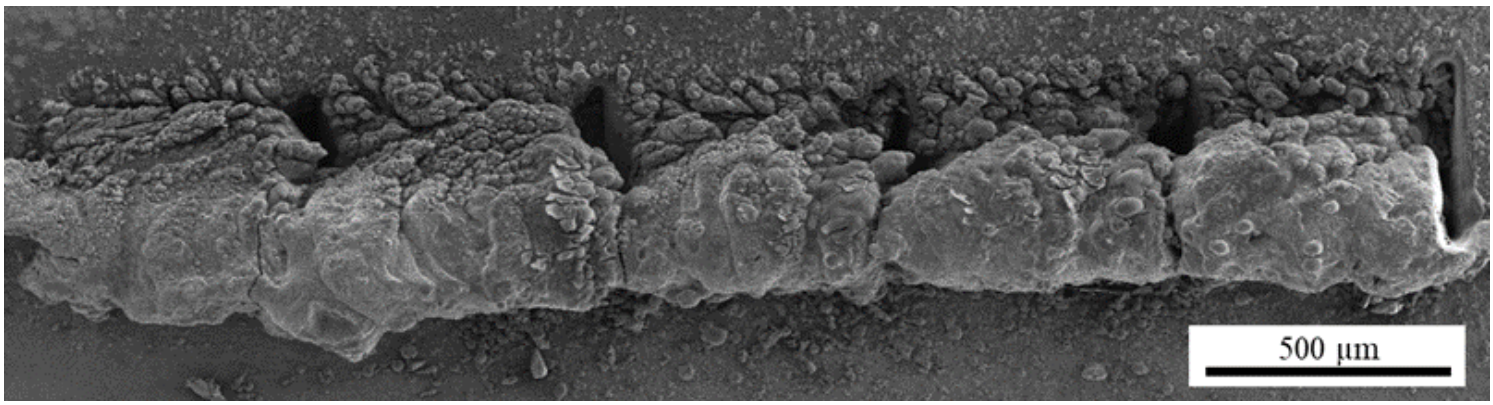

Figure 5

Example of the accumulation of material inside a groove when high laser energy is used (P = 100 %, s = 100 mm/s, n = 128).

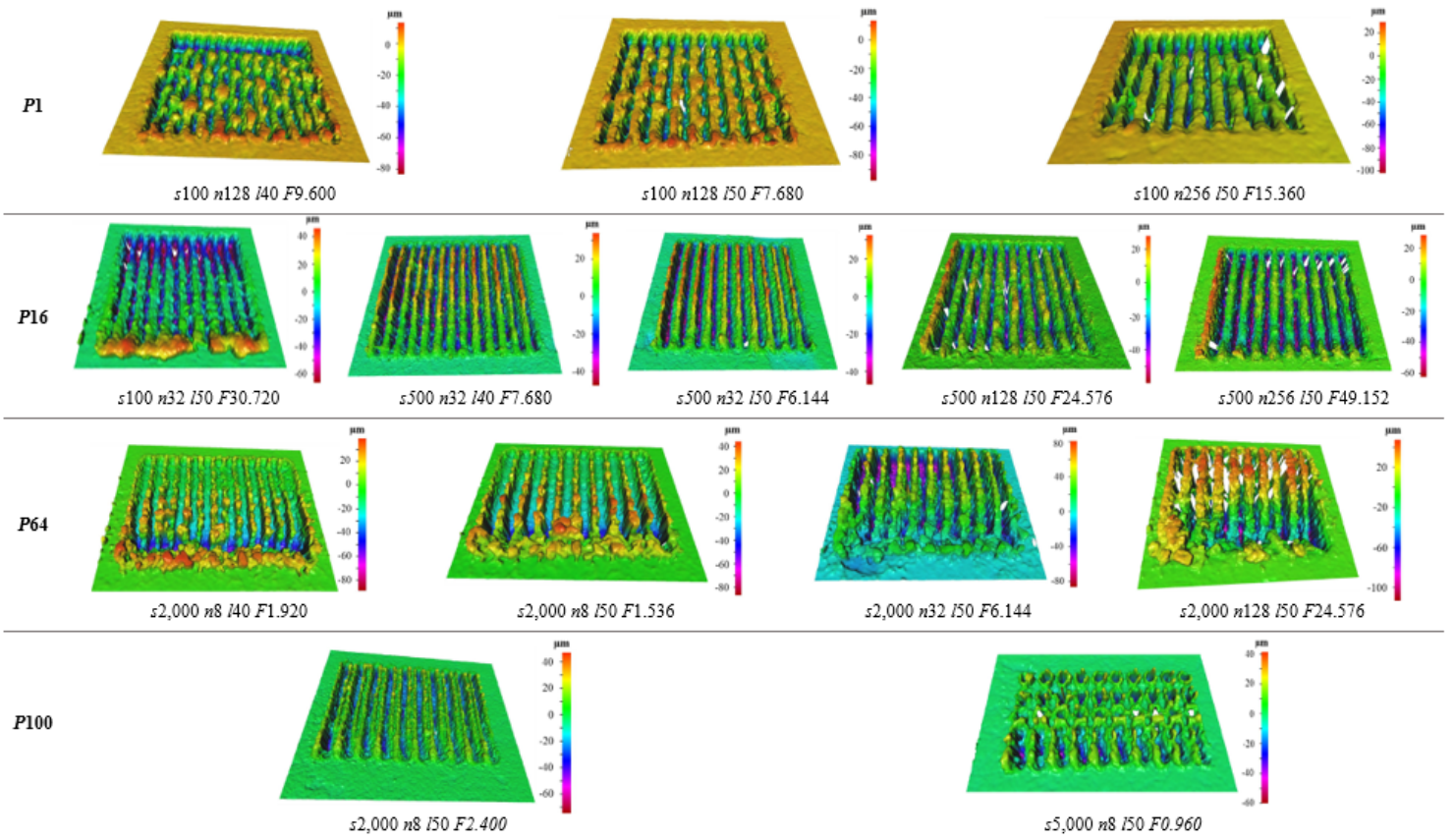

Figure 6

Profile heights of the most promising textures (P = laser power in %, s = scanning speed in mm/s, n = number of passes, l = line spacing in µm, and F = laser energy fluence in J/mm^2)

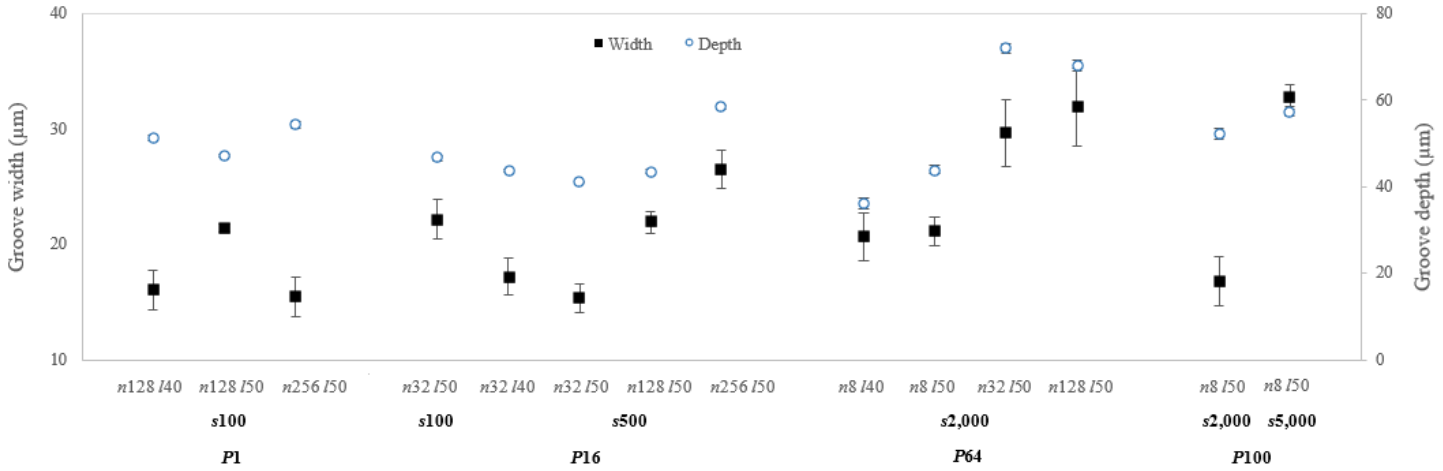

Figure 7

Width and depth in the middle of the textured grooves obtained from different combinations of parameters.

(*P* = laser power in %, *s* = scanning speed in mm/s, *n* = number of passes, *l* = line spacing in µm)

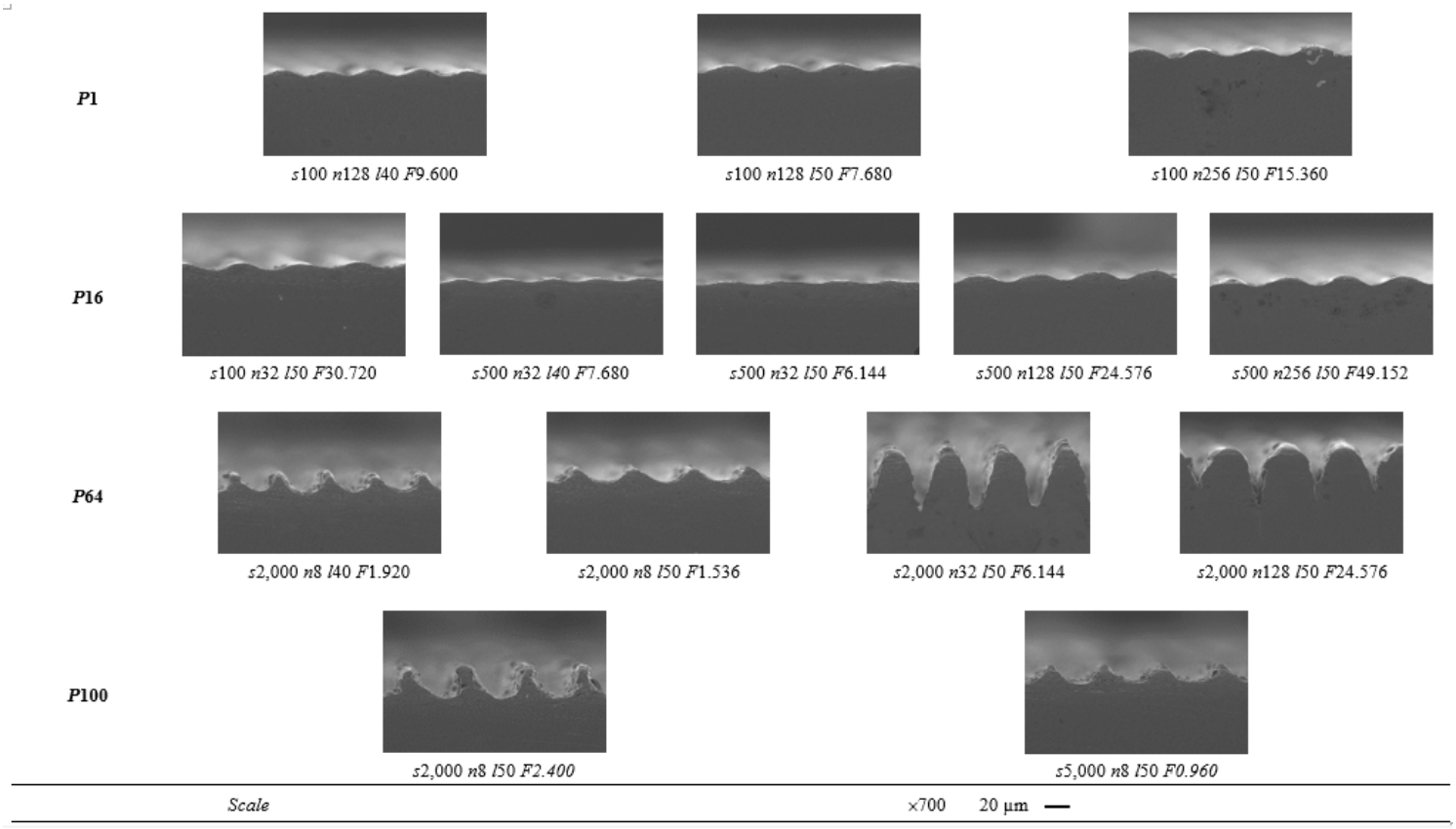

Figure 8

SEM images of the cross-sections of the fourteen samples with the most promising textures (P = laser power in %, s = scanning speed in mm/s, n = number of passes, l = line spacing in µm, and F = laser energy fluence in J/mm^2).

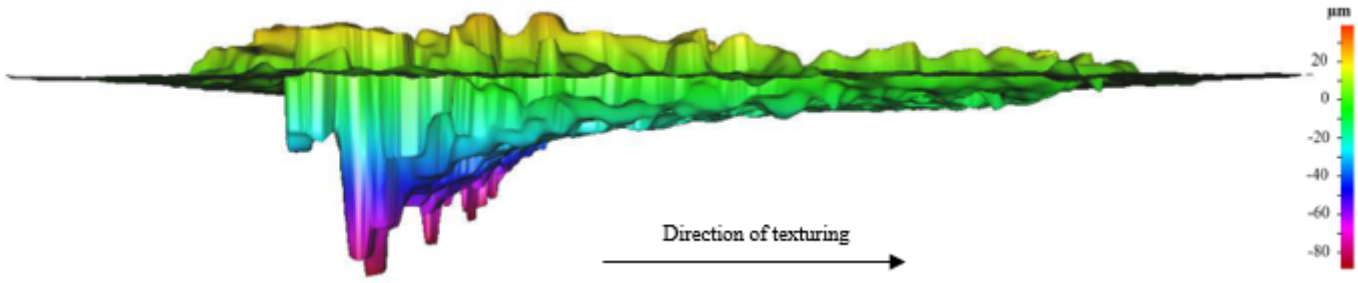

Figure 9

Depth profile of the 420 stainless steel textured with P = 64 %, s = 2,000 mm/s, n = 8, l = 40 µm,.

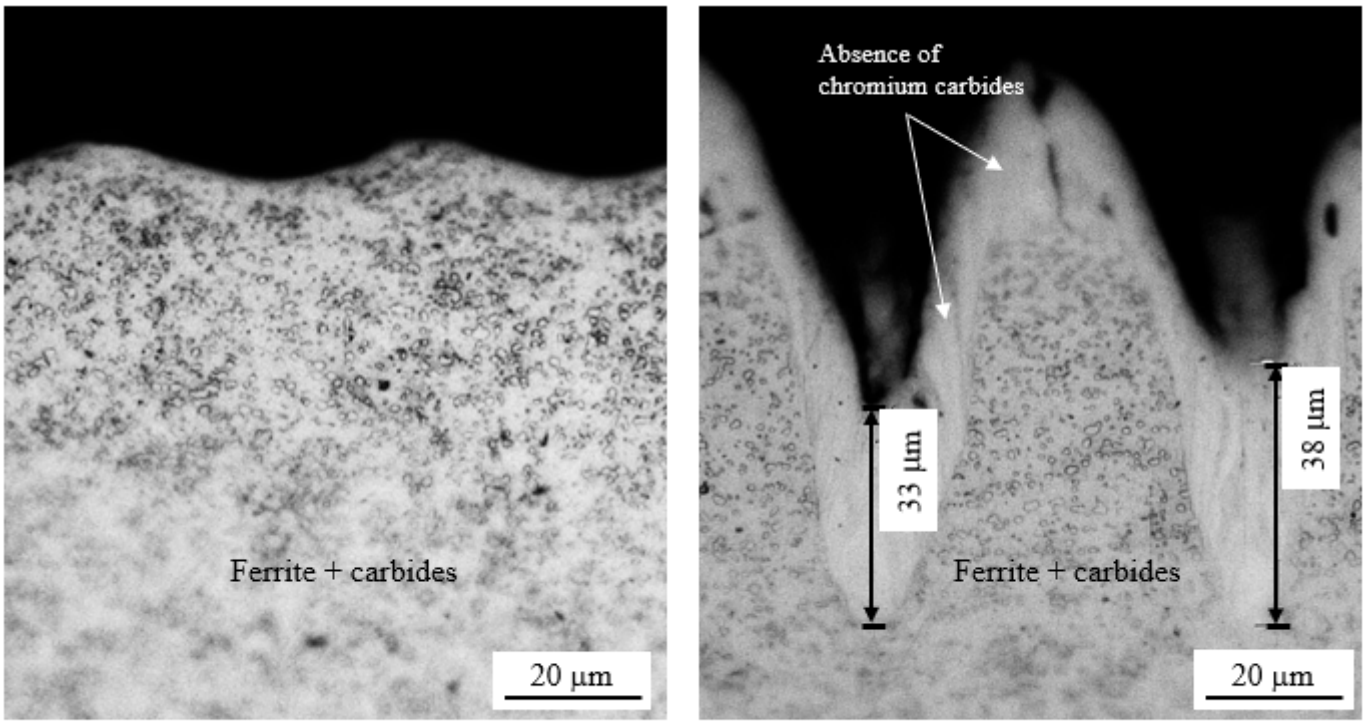

Figure 10

Typical examples of the microstructure of 420 stainless steel after texturing using (a) low laser power and scanning speed (P = 16 %, s = 500 mm/s, n = 256) and (b) high laser power and scanning speed (P = 64 %, s = 2,000 mm/s, n = 32). The line spacing in both cases was 50 µm.